Journal of Information Display, vol. 2, no. 3, 2001

Infrared Spectroscopic Study of Molecular Hydrogen Bonding in Chiral Smetic Liquid Crystals

Won Gun Jang

Abstract

We utilize Fourier transform infrared (IR) spectroscopy to probe intramolecular hydrogen bonding in smectic-C* liquid crystal phases. Infrared spectra of aligned smectic liquid crystal materials vs. temperature and of isotropic liquid crystal mixtures vs. concentration were measured in homologs, both with and without hydrogen bonding. Hydrogen bonding significantly changes the direction and magnitude of the vibrational dipole transition moments, causing marked changes in the IR dichroic absorbance profiles of hydrogen bonded molecular subfragments. A GAUSSIAN94 computation of the directions, magnitudes, and frequencies of the vibrational dipole moments of molecular subfragments shows good agreement with the experimental data. The results show that IR dichroism can be an effective probe of hydrogen bonding in liquid crystal phases.

Keywords : smectic liquid crystal, fourier transform infrared spectroscopy(FT-IR), IR dichroism, hydrogen bonding.

1. Introduction

Hydrogen bonding (H-bonding) is one of the key attractive interactions stabilizing condensed phases and promoting molecular self assembly. The effects of H-bonding in liquid crystal forming materials is of particular interest. For example, molecules incapable of mesogenic ordering can H-bond into larger units which do possess liquid crystal phases. Many studies of the role of H-bonding in the formation and stabilization of liquid crystals have been carried out, ranging from the development of the classic Sm-C phases formed from benzoic acid dimers [1], to more recent studies of the effects of inter- and intramolecular H-bonding on LC phase stability [2, 3]. More efforts have been made recently to utilize intra-molecular H-bonding to enhance spontaneous ferroelectric polarization, **P**, in chiral smectic-C* (Sm-C*) phases [4], based on the intuition that H-bonding would align the dipole moments of a carbonyl group and of a hydroxyl substituent on a phenyl ring into the same direction. In another recent study on LC-forming dimers having a bent (banana) shape have been prepared by complexation of phthalic or isophthalic acid and two molecules of stilbazole through intermolecular H-bonding [5]. It has also been reported that the mesogen formed by the H-bonding between chiral mono-(2-methylbutyl)-ester of terephthalic acid and 4-alkoxy-4'-stilbazole homologues has blue phases, that is the chiral nematic (N*) phase, and the Sm-C* phases [6].

Infrared dichroism is considered to be an especially powerful way of probing molecular ordering in LC phases. This is because the orientational ordering of molecules in LCs makes the polarization dependence of the absorbance of infrared light by molecular vibrations an effective tool for probing molecular organization. In this paper we use IR dichroism to study LCs which involves H-bonding. Some examples that H-bonding significantly alters the interpretation of IR dichroism

Manuscript received August 7, 2001; accepted for publication August 21, 2001.
This work supported by NSF MRSEC GRANT DMR 98-09555.
Corresponding Author : Won Gun Jang
Korea Photonics Technology Institute(KOPTI) 459-3 Bonchon-dong, Buk-gu, Kwangju 500-210, Korea.
E-mail : wgjang@kopti.re.kr **Tel** : +62 573-8684 **Fax** : +62 573-1616

data. We studied several chiral Smectic-A* (Sm-A*) and Sm-C* liquid crystals, comparing the behavior of molecular homologs which differ only by a single H-bonding moiety. We probe the vibrational transition moment orientations of the phenyl rings, the C=O groups, and the H-bond-inducing OH and NH groups within molecules, as well as the molecular orientation and conformation distribution in the smectic phases. Temperature and concentration of H-bonding species are key parameters in these experiments, because H-bonds can be expected to be broken thermally or by dilution of H-bonding molecules. Wavenumber shifts as well as changes in band intensity and shape are analyzed in terms of variations of intra- and inter-molecular H-bonding [7]. Observed transition moment frequencies, directions and magnitudes are calculated using Gaussian94 computational chemistry tools for comparison with the data.

2. Experiments

2.1 IR dichroism

The experimental cell geometry is shown in Fig. 1. The LC samples were homogeneously aligned in IR transparent capacitors made from CaF_2 windows coated with a 100 Å-thick layer of indium tin oxide (ITO) for electrodes and 200 Å thick rubbed nylon alignment layers. Alignment quality was checked with visible light polarized microscopy. The layer structure obtained upon cooling into the Sm-C* phase was chevron, but the voltage threshold for deforming the chevron structure into the bookshelf was quite low (several volts), so that the IR experiments were always carried out in the bookshelf geometry, i.e., with the smectic layers normal to the plates. The spacing between the plates was 2 ~ 3 μm, maintained by spacers. IR light was incident normal to the cell plates and linearly polarized in the **y-z** plane at an angle Ω relative to the layer normal **z**, Ω being determined by a wire-grid IR polarizer orientation. Vibrational absorption peaks were background subtracted and fit, based on the Levenberg-Marquardt algorithm, to combination of Gaussian and Lorenzian functions to determine the peak absorbances of vibrations of interest [8].

In order to extract vibrational moment and molecular orientation parameters from IR dichroism data it is necessary to measure absorbance vs. polarizer orientation Ω for the full range of Ω [9,10]. Ignoring birefringence [11], A(Ω) for any mode is a universal function of three parameters, that is the absorbances A_{para} (A_{perp}) measured with the IR polarizer parallel (perpendicular) to the $\Omega_o = 0$ axis, the polarizer orientation for either maximum (A_{max}) or minimum (A_{min}) absorbance

$$A(\Omega) = -\log\{(10^{-A_{para}})\cos^2(\Omega - \Omega_o) + (10^{-A_{para}})\sin^2(\Omega - \Omega_o)\}. \quad (1)$$

Thus, Eq (1) obtains for A(Ω) no matter what the molecular orientation distribution, with the three parameters A_{max}, A_{min}, and Ω_o related to the three moments, $\langle p_y^2 \rangle$, $\langle p_z^2 \rangle$ and $\langle p_y p_z \rangle$, of the absorption dipole **p**. Dichroism D is defined as $D \equiv A_{max}/A_{min}$ and can be a good order parameter.

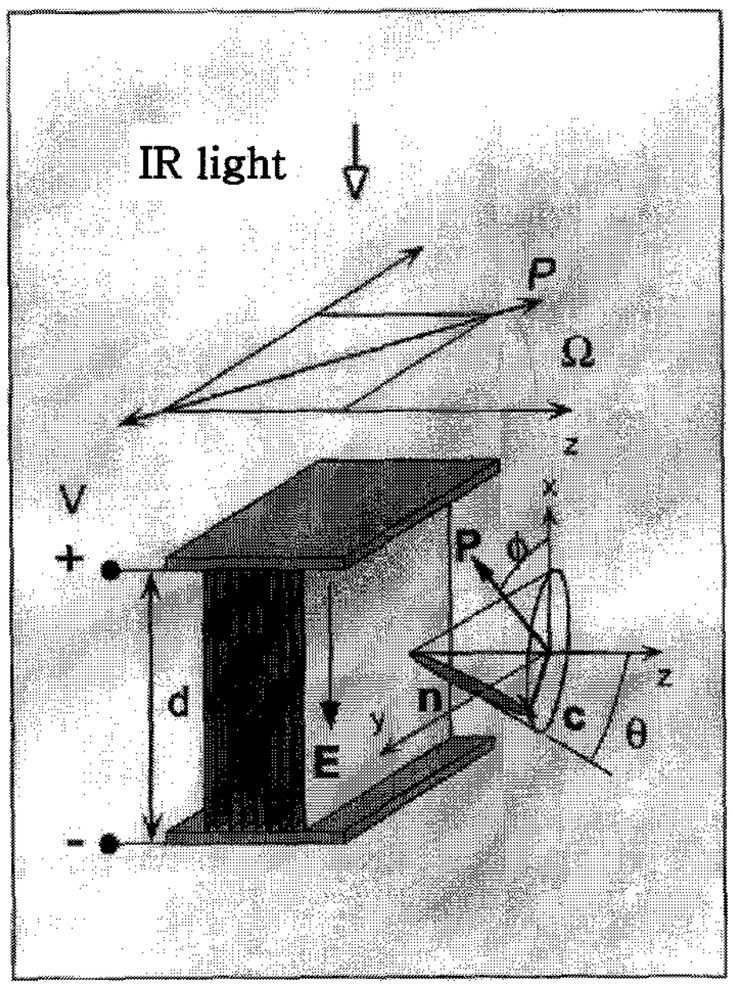

Fig. 1. A schematic diagram of the FTIR experiment.

2.2 Liquid crystal materials

The ferroelectric liquid crystal materials used in this study and their phase diagrams are shown in Fig. 2. The materials have been designed and synthesized in an effort to obtain ferroelectric Sm-C* LCs, and, indeed, all of them have the Sm-C* phase, as well as the Sm-A*. The compounds NTT-noOH and NTT-OH [12] differ only by the lateral OH substitution on the core phenyl.

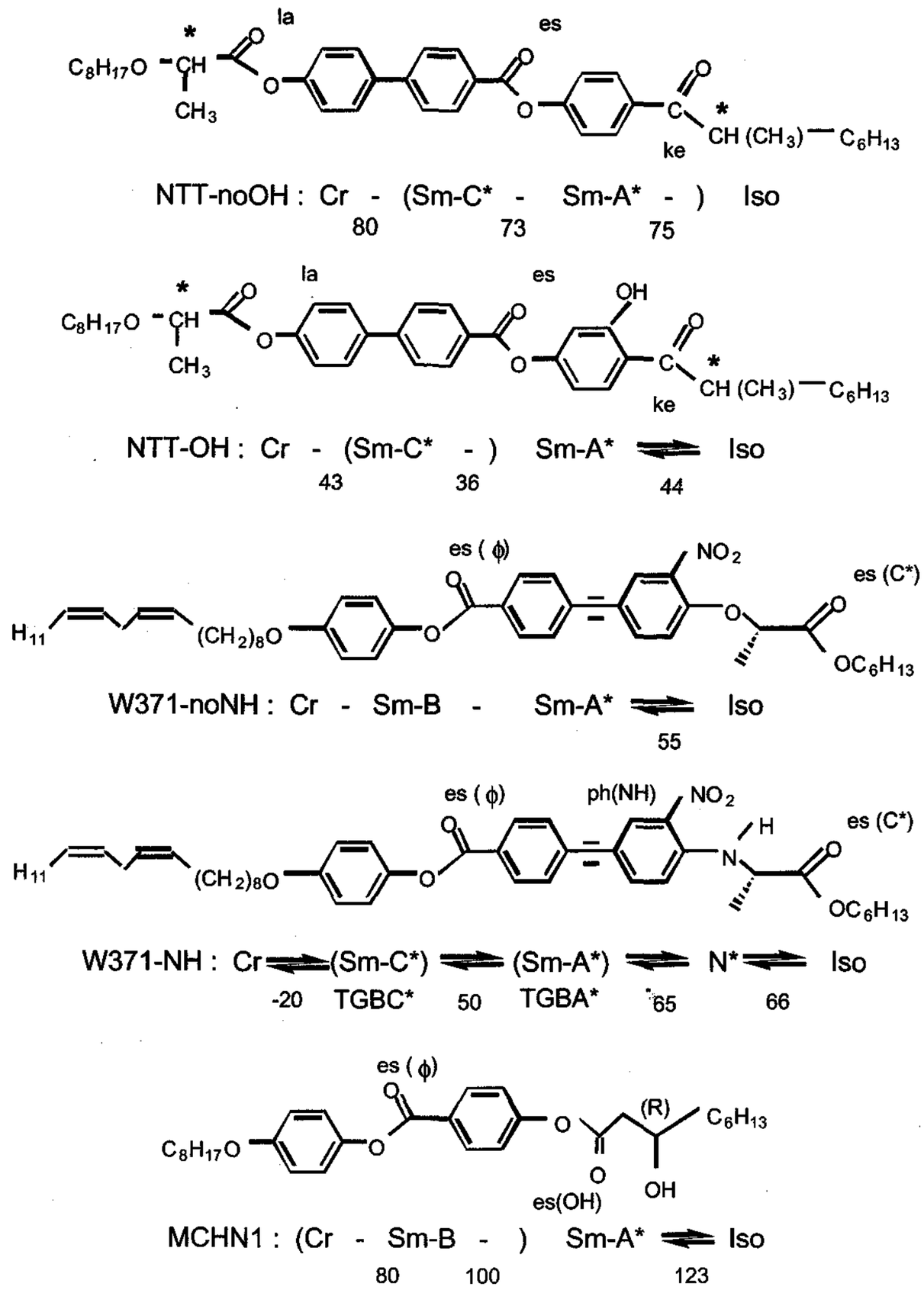

Fig. 2. Liquid crystal materials used in these experiments and their phase diagrams.

W371-NH was designed for large nonlinear susceptibility by introducing the NO_2 on the core phenyl and has a high Sm-C* P = -19.7 nC/cm^2 at 40 °C as a result of the NO_2 dipole. Because of the tolane group the W371 family has a tendency to form TGB phases, with W371-NH having both TGBA and TGBC. In the CaF_2 IR cells, application of a few volts unwinds the TGB helix and establishes bookshelf alignment. [13]. W371-noNH has no Sm-C phase. MCHN1 has Sm-A and Sm-B phases.

2.3 Dichroism experiments

In order to extract vibrational moment and molecular orientation parameters from IR dichroism data, A(Ω) was obtained by fits to the spectra for a series of Ω, spaced by 10° intervals over 360°. The results are displayed in Fig. 3-5 as polar plots of peak absorbance A(Ω), which effectively exhibit the dichroism of each mode.

2.3.1 NTT compounds

Fig. 3. shows dichroism data A(Ω) of several molecular vibration bands of the two NTT compounds in the Sm-A* phase (T = 39 °C). These materials possess three C=O groups whose stretching vibrations are distinguishable in the IR spectra. The A(Ω) for these and the phenyl stretching peak are shown in Fig. 3 (ke, keto carbonyl; es, ester carbonyl; la, lactic carbonyl; ph, phenyl), where the different C=O groups are indicated in Fig. 2.

2.3.2 NTT-noOH

A(Ω) observed can be qualitatively understood for

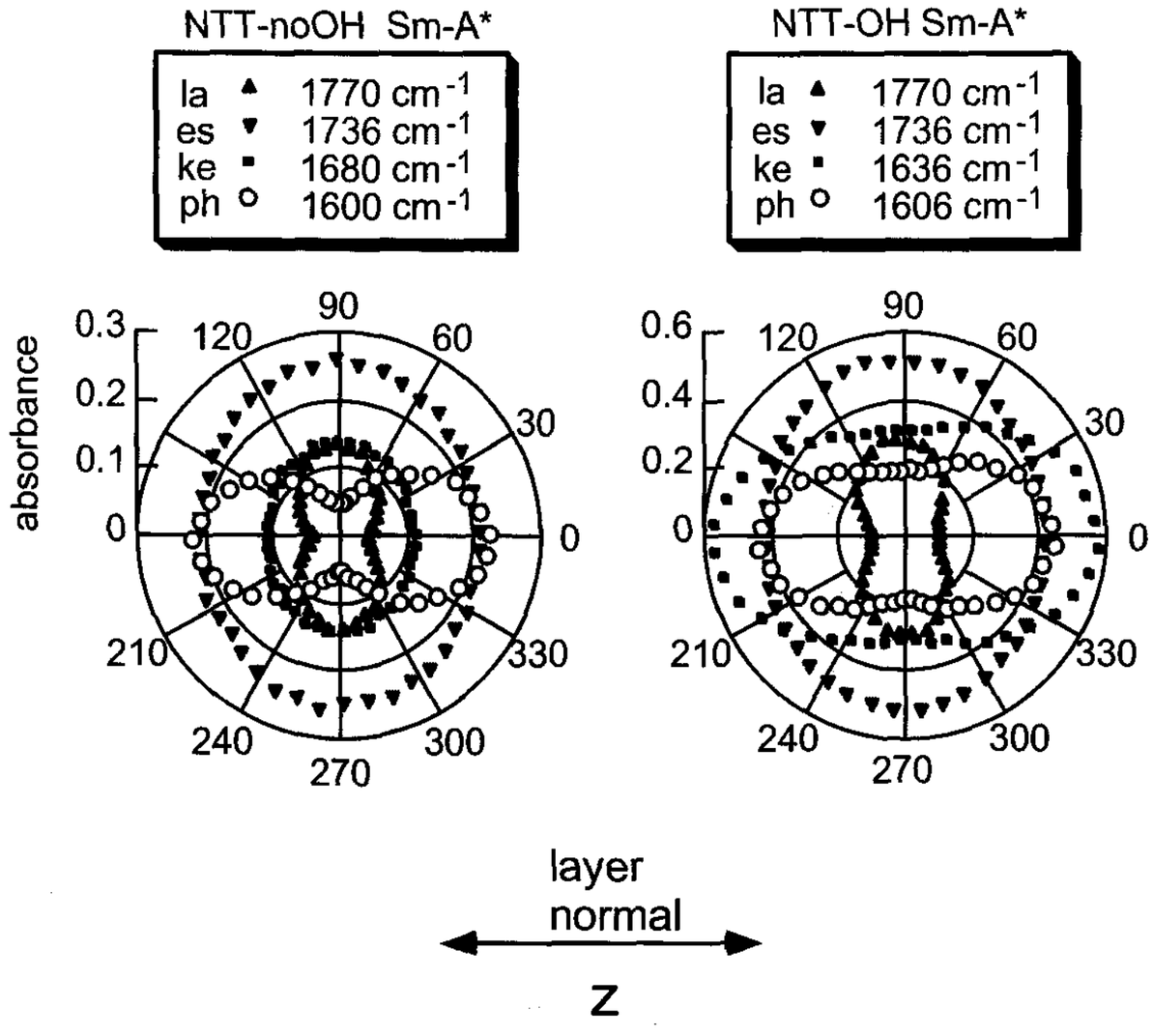

Fig. 3. Polar plot of absorption profiles for phenyl and C=O stretching vibrations in the NTT compounds. The keto (ke) C=O peak at 1636 cm^{-1} shows abnormal dichroism with the OH substitution on the phenyl ring, with maximum absorbance for polarization parallel to the layer normal. The lactic (la) and ester (es) C=O and phenyl (ph) absorbance data are also shown.

each mode in terms of β, the angle between its absorption dipole and the molecular long axis In NTT-noOH, the phenyl core vibration has $\beta_{phenyl} \sim 0°$, and thus, the largest change in absorbance (dichroic ratio $D \equiv A_{max}/A_{min}$ ~4.25 with maximum at $\Omega = 0°$). The NTT-noOH carbonyl stretching vibrations, with β in the range $60° < \beta < 80°$, show behavior typical of non-H-bonded Smectic-A materials. They have a smaller dichroic ratio ($D < 2$) than the phenyl, and have A_{max} at $\Omega = 90°$, both because of the proximity of β to the "magic angle", $\beta = 54.7°$, for which a uniaxial distribution around the long axis appears isotropic ($D = 1$ for $\beta_{magic} = 54.7°$) and because A_{max} is at $\Omega = 90°(0°)$ for $\beta >(<) \beta_{magic}$. The **la** C=O has the largest β ($\beta_{la(C=O)} \sim 80°$) and thus D_{la} is the largest of the dichroic ratios of the carbonyls.

2.3.3 NTT-OH

NTT-OH exhibits a dichroism pattern which is similar to that of the NTT-noOH, with the exception of a dramatic difference for the (**ke**) C=O near the OH ($D_{ke(C=O)} = 1.86$). Specifically, the NTT compound *with* the OH group on the phenyl ring exhibits A_{max} for the **ke** C=O group at $\Omega = 0°$, rather than $\Omega = 90°$ for the NTT-noOH. Furthermore, even though the molecular shape has hardly changed, the dichroic ratio of the phenyl stretching peak decreases to $D_{ph} = 2.31$, i.e., indicating either a decrease in order parameter or a reorientation of the absorption dipole relative to the long molecular axis, i.e., an increase of β_{ph}. Dichroism data for the OH stretching vibration was not obtainable because of overlap with the CH stretching peaks.

2.3.4 W371 compounds

Remarkable IR dichroism behavior, illustrated in Figure 4, was also observed for the C=O vibrations in the Smectic-A phase of the W371 compounds, as follows.

2.3.5 W371-noNH

The carbonyl and phenyl absorbance profiles of W371-noNH look quite as expected, with A_{max} at $\Omega = 0°$ for the phenyl and at $\Omega = 90°$ for the **es**(ϕ) carbonyl at 1736 cm^{-1} and the **es**(C^*) carbonyl at 1756 cm^{-1}.

2.3.6 W371-NH

In W371-NH, the peak from the **es**(C^*) C=O group at 1756 cm^{-1} disappears, and small peaks at 3370 cm^{-1} and 3347 cm^{-1} appear, assignable to a H-bonded NH group. In addition, a high dichroic ratio peak (D ~ 4.91 at

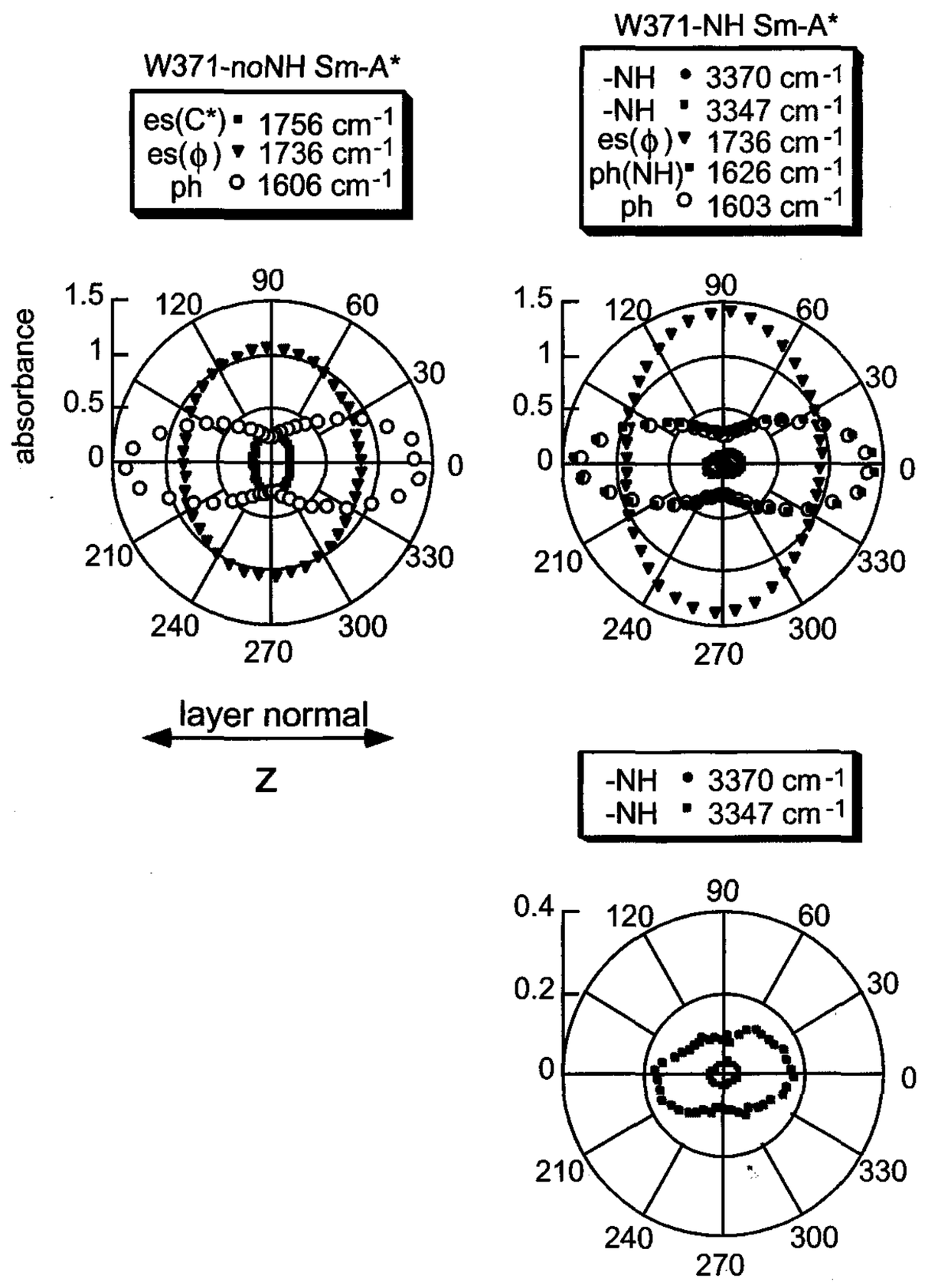

Fig. 4. Polar plot of absorbance profiles of the W371 compounds. The 1756 cm^{-1} C=O peak disappears upon introduction of NH, shifted down in wavenumber to overlap the 1736 cm^{-1} peak, increasing its dichroism.

1626 cm^{-1}) with A_{max} at $\Omega = 0°$ appears and the **es**(ϕ) C=O (1736 cm^{-1}) dichroic ratio apparently increases from $D_{es} = 1.28$ to $D_{es} = 1.53$.

2.3.7 MCHN1 compound

In Smectic-A MCHN1, peaks from the two C=O groups were observed, **es**(ϕ) at 1730 cm^{-1} and **es**(OH) at 1765 cm^{-1}, a high dichroic ratio phenyl peak (D_{ph} = 7.87), and also two small but distinct OH peaks (3470 cm^{-1} and 3560 cm^{-1}), having A_{max} at $\Omega = 90°$, as illustrated in Fig. 5.

2.4 Dilution and temperature scan experiments

Dilution experiments for further study of H-bonding effects were carried out, dissolving the NTT-OH and W371-NH compounds at low concentration in carbon tetrachloride (CCl_4), which has no H-bonding interactions. MCHN1 did not readily dissolve in the available non-polar, non-H-bonding solvents, so its H-bonding characteristics were studied by varying temperatures, T. Results of these experiments are as follows.

2. 4. 1 NTT-OH

Particular attention was paid to the OH stretching peak, expected to have a wavenumber k in the region 2500 $cm^{-1} < k < 2900$ cm^{-1} when H-bonded, and $k \approx$ 3500 cm^{-1} when not H-bonded [15]. The NTT-OH/CCl_4 spectra in Fig. 6. show no signal for k ~3500 cm^{-1} no matter how much NTT-OH is diluted, but show

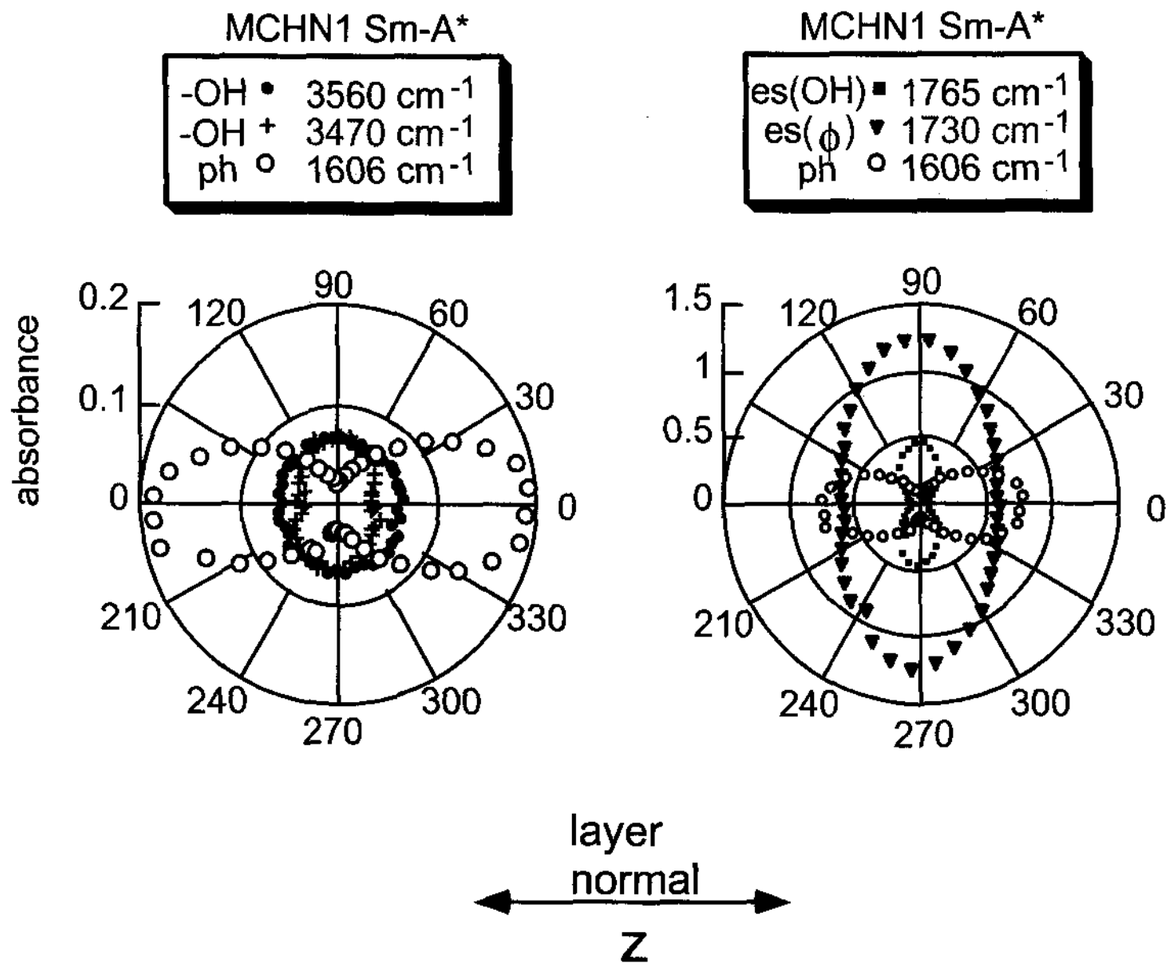

Fig. 5. Polar plot of absorbance of MCHN1. There are two OH peak frequencies, 3470 and 3560 cm^{-1}, for molecules with stronger and weaker H-bonding, respectively.

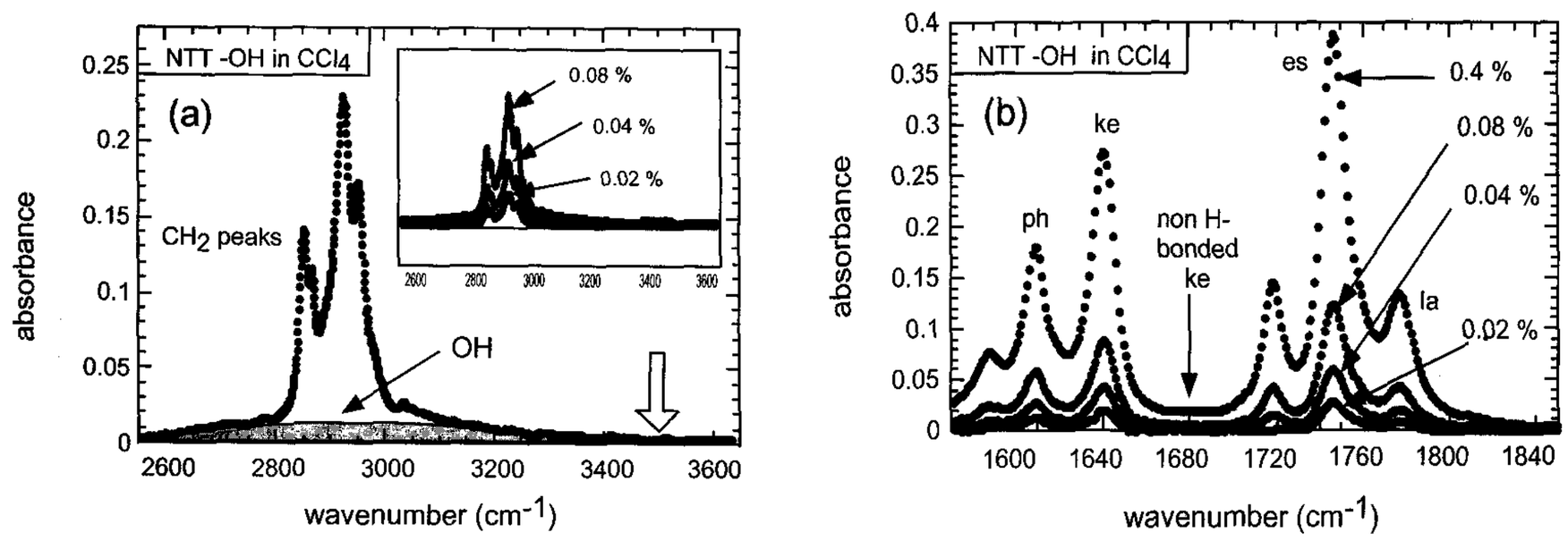

(a) (b)

Fig. 6. Results of the dilution experiment for NTT-OH in CCl_4. (a) The OH peak with strong H-bonding overlaps the CH_2 peaks. The non-H-bonded OH stretching peak, expected at the white arrow, is absent. (b) The C=O frequencies are independent of concentration, with frequencies indicating no H-bonding for the **es** and **la** and strong H-bonding for the **ke**, the 1680 cm^{-1} non H-bonded **ke** peak being absent.

a broad peak for k ~2900 cm^{-1} overlapping the CH stretching peaks, which is not observed in the absence of OH. This dilution experiment clearly shows that the OH group undergoes strong concentration independent, and therefore *intramolecular* H-bonding, which can occur only for the **ke** C=O. Consistent with this is the observation that the wavenumbers of the three C=O groups, in particular the **ke** carbonyl, are not shifted at all upon dilution. Furthermore, the **ke** C=O stretching frequency is found at 1636 cm^{-1}, the frequency range expected when H-bonded, and that there is no sign of a non-H-bonded **ke** carbonyl peak, expected at k ≈ 1680 cm^{-1} from the spectra of NTT-noOH.

2.4.2 W371-NH

Fig. 7. shows spectra in the NH stretching region of W371-NH, both for the neat compound in the Sm-A phase, and under various conditions of dilution in CCl_4. The NH stretching frequency is expected to be 3340 cm^{-1} when H-bonded and 3370 cm^{-1} when not H-bonded. The NH peak, at k ≈ 3340 cm^{-1} in the neat Sm-A, is split into two peaks in solution, shifted up in wavenumber to

$k \approx 3347\ cm^{-1}$ and $k \approx 3370\ cm^{-1}$. These peak positions and relative intensities are independent of W371-NH concentration, indicating that there are two distinct modes of intramolecular H-bonding in solution, the weaker giving the larger shift. The **ph**(NH) wavenumber is independent of concentration, also indicative of intramolecular H-bonding. The **es**(ϕ) C=O wavenumbers are independent of concentration, as expected since this C=O is not involved with H-bonding. In W371-NH, the **es** (NH) C=O stretching frequency is expected to be $1626\ cm^{-1}$.

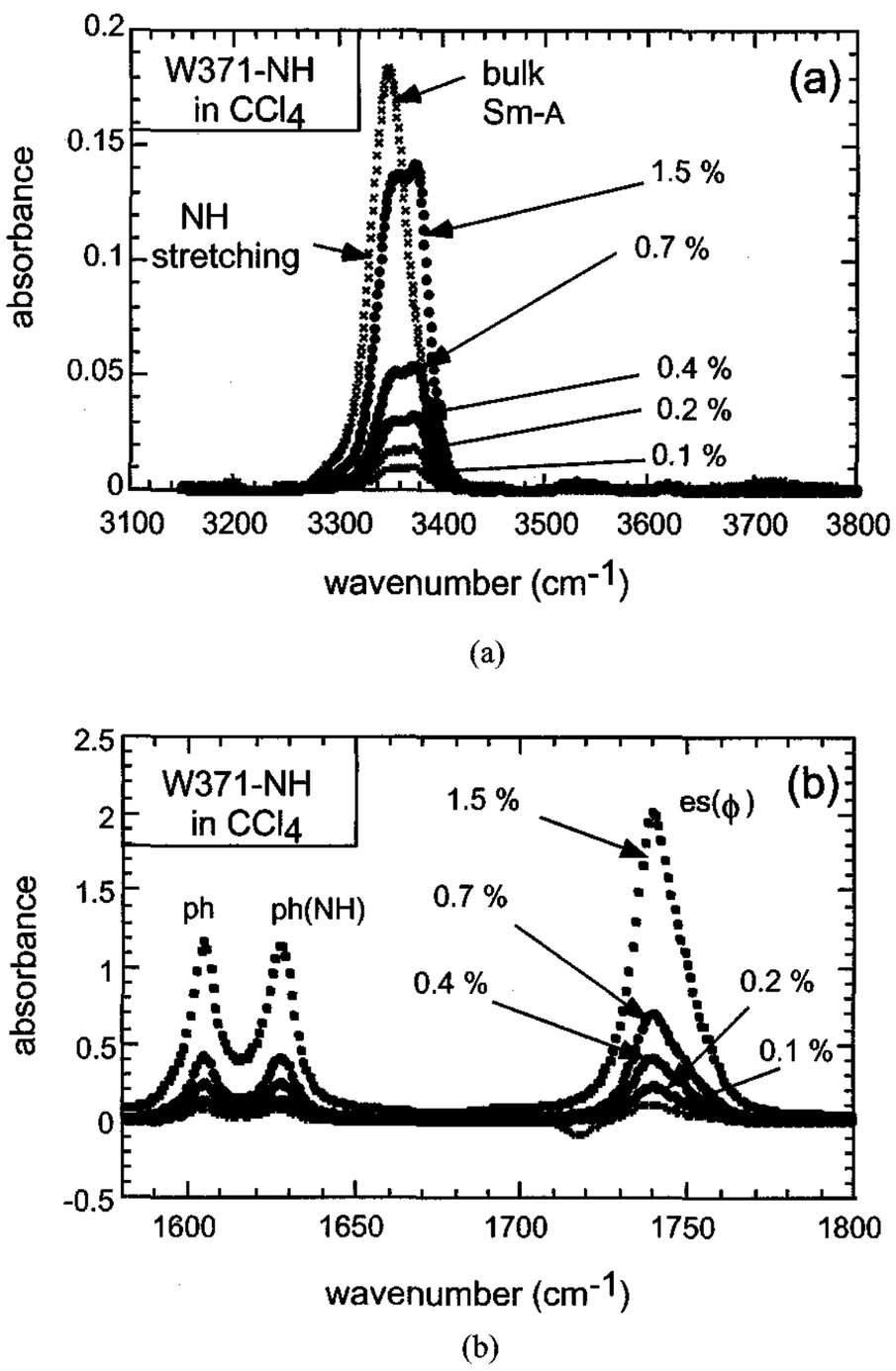

Fig. 7. Results of the dilution experiment for W371-NH in CCl_4. (a) The split NH peak indicates two kinds of H-bonding: the strongly H-bonded NH peak at ~3347 cm^{-1} and the weakly H-bonded NH stretching peak at ~3370 cm^{-1}. (a,b) The concentration independence of the NH and ph(NH) wavenumbers indicates intramolecular H-bonding.

2.4.3 MCHN1

T scans showed bimodal intensity distributions for both the OH and **es**(OH) C=O regions, with low T wavenumbers ($k_{OH} \approx 3440\ cm^{-1}$, $k_{C=O} \approx 1735\ cm^{-1}$) indicating an OH - C=O H-bond. These peaks decrease and non-H-bonding peaks grow for both regions with increasing T (Fig. 8.)

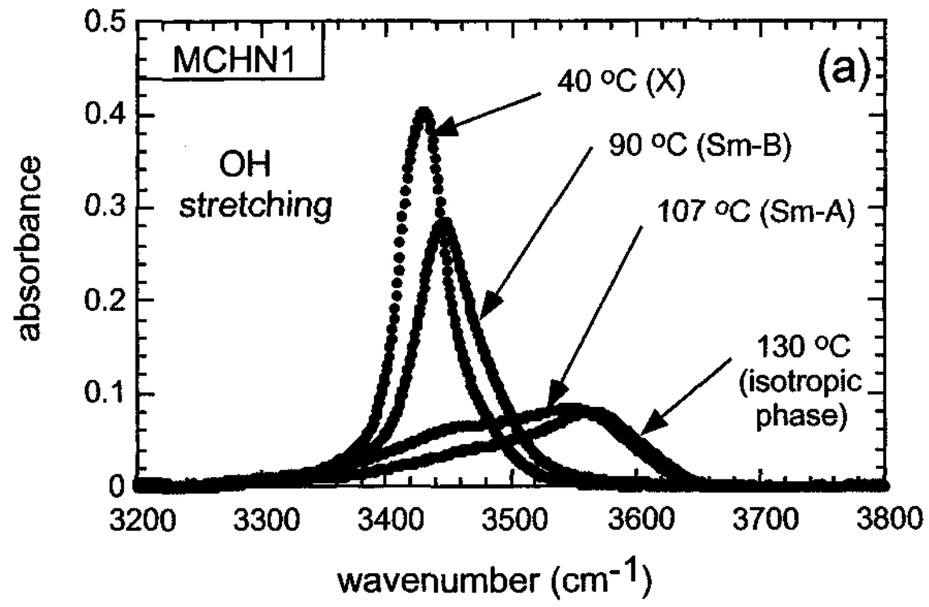

Fig. 8. Results of the temperature scan experiment of MCHN1. Both the OH and **es**(OH) peaks show evidence for a T-dependent OH-C=O H-bond, evolving from H-bonded wavenumbers at low T (3440 cm^{-1} and 1740 cm^{-1} respectively) to split peaks at high T, with non-H-bonded peaks (3560 cm^{-1} and 1765 cm^{-1}) appearing.

2.5 Calculation of wave numbers and transition moments

In order to understand the dependence of the molecular structure and transition moment directions on H-bonding, and to assist in assigning spectral features, we carried out density functional theory (DFT) calculations of vibration wavenumbers and transition moment magnitudes and directions using Gaussian94 [16,17]. In DFT the total energy is a functional of the atomic electron density, expressed as basis set of functions. The basis set used here, 6-31G* (or 6-31G(d)), is comprised of six Gaussian functions for the atomic core orbitals, and three inner and one outer Gaussian function for the atomic valence orbitals. The "*" indicates that a set of d-functions was added for each

Table 1. Experimental and calculated wavenumbers (cm^{-1}).

NTT compounds		**Experimental**	**Calculated**
keto C=O [ke]	w/o OH	1680	1697
	with OH	1636	1638
ester C=O [es]	w/o OH	1736	1742
	with OH	1736	1745
lactic C=O [la]	w/o OH	1770	1760
	with OH	1770	1760
OH	w/o OH	na	na
	with OH	2900	3137
phenyl [ph]	w/o OH	1600	1594
	with OH	1606	1605
W371 compounds		Experimental	Calculated
ester C=O [es]	w/o NH	1736	1736
	with NH	1736	1736
Eester C=O [es(C*)]	w/o NH	1756	1763
	with NH	1736	1745
NH	w/o NH	na	na
	with NH	3347	3351
		3370	3367
phenyl [ph]	w/o NH	1600	1600
	with NH	1600	1605
phenyl [ph(NH)]	with NH	1560	1549
			1570
		1626	1617
MCHN1 compound		Experimental	Calculated
ester C=O [es(OH)]	with H-bond	1730	1722
	w/o H-bond	1765	1758
OH	with H-bond	3470	3560
	w/o H-bond	3560	3571
phenyl [ph]	with H-bond	1600	1600
	w/o H-bond	1600	1605

non-hydrogen (heavy) atom. The molecular orbitals are constructed by a linear combination of the atomic orbitals. Electron correlation was incorporated using the Becke3LYP (B3LYP) correlation functional, which is Becke's three parameter hybrid variant of the Lee, Yang, and Parr correlation functional [18,19]. The CPU time

requirements and performance of DFT calculations depends not only on the size of the chemical system, but also on the "tightness" of the integration grid, smaller grid spacing giving more accurate energies and electron density. Limits set by finite computational resources required calculations to be carried out only on fragments of the LC molecules. The fragments chosen were the smallest molecular entities incorporating all electrons having significant correlations with those of interest, and the grid spacing chosen for a particular molecular fragment was the smallest consistent with available CPU time. Relative energies of conformations of particular fragments were always compared with the same grid spacing [20]. Vibration frequencies and transition moments were calculated by Gaussian94 with Ampac graphic interface. Calculated wavenumbers were scaled by a factor of 0.9613, appropriate for the B3LYP/6-31G* level [16].

Table 1 shows the calculated wavenumbers for the vibrations under study along with experimental values obtained in the Sm-A phase of the neat compounds. The correlations between calculated and measured wavenumbers is generally quite good, and reveals significant effects of H-bonding, as discussed in the previous sections and below.

3. Discussion

3.1 NTT compounds

The most striking observation in the NTT compound spectra was the 90° change in the Ω of A_{min} in A(Ω) of the **ke** carbonyl upon introduction of the OH phenyl ring substitution. This change indicates that the dipole transition moment direction of **ke** C=O is rotated significantly (by more than 30°) toward the molecular long axis upon H-bonding. furthermore, the vibration wavenumber of this carbonyl undergoes a big shift, from 1680 cm^{-1} to 1636 cm^{-1} and the dichroic ratio of the phenyl peak (1606 cm^{-1}) decreases to $D_{1606} \sim 2.31$. These changes can be understood on the basis of the computed transition moments in the NTT compounds' molecular fragments shown in Fig. 9. The vibration wavenumber calculation yields a **ke** carbonyl wavenumber shift from 1697 cm^{-1} (-noOH) to 1638 cm^{-1} (with OH), and a change in the transition moment direction to $\beta_{C=O} = 25°$, for which we expect D = 2.73 [11] and A_{max} for Ω = 0°, as observed. The two **es** carbonyl frequencies are independent of the presence of the OH group para to the ester, in agreement with experiments.

The phenyl group frequencies are not changed by the presence of the OH, in agreement with experiments. Furthermore, the calculated β_{phenyl} increases to β_{phenyl} =45°, which is the cause for the decrease of D_{1606}. β_{phenyl} =45° yields a D_{phenyl} = 1.6 for the absorbance of the phenyl which, when added to the absorbance of the biphenyl ($D_{biphenyl}$ = 4.25 from the NTT-noOH data), yields a decrease in the apparent D of the 1606 cm^{-1} peak to D_{1606} = 2.8, as shown in Figure 10. This is close to the observed D_{1606} = 2.31.

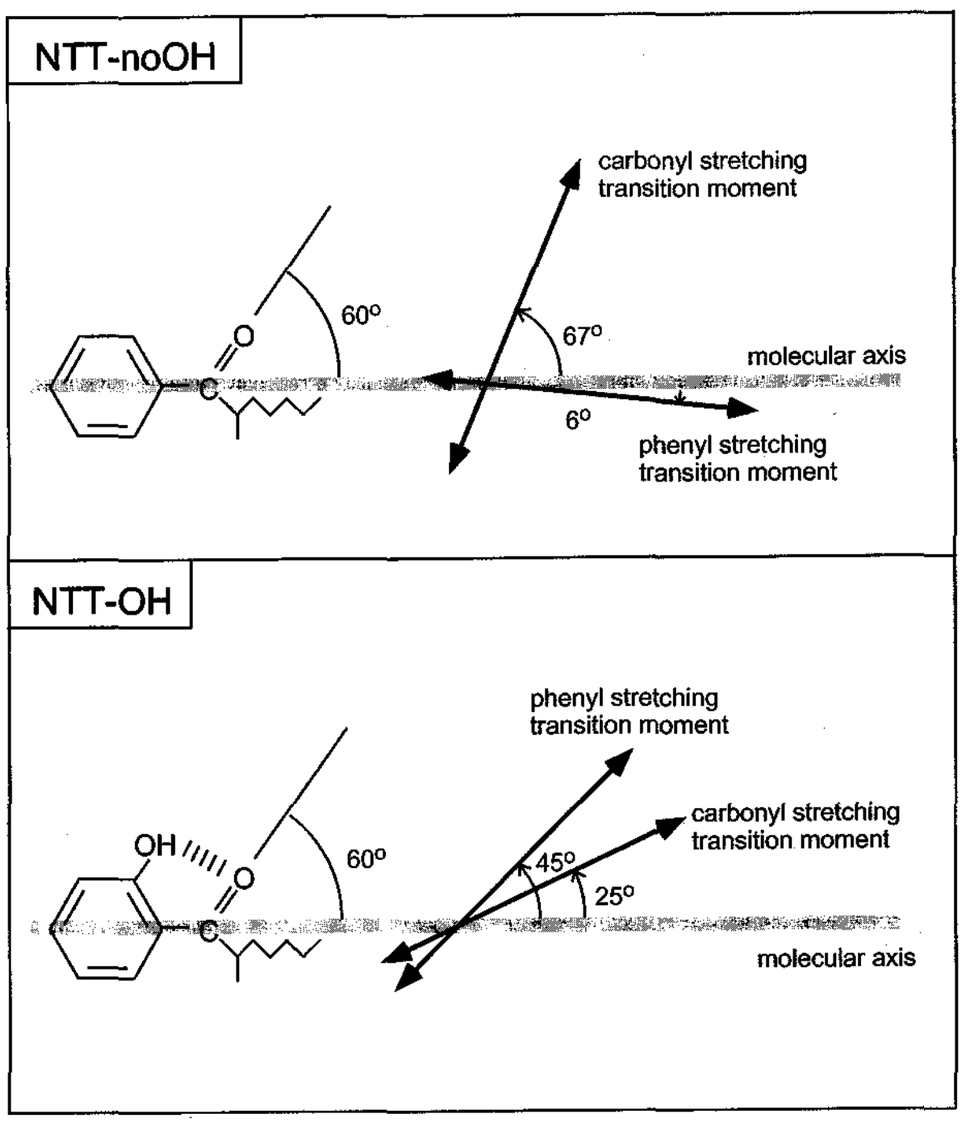

Fig. 9. Transition moment directions calculated for NTT-OH and NTT-noOH fragments, showing the effect of the OH substitution and OH-C=O H-bonding. (a) The noOH orientations are quite typical. (b) H-bonding shifts the transition moment direction of the C=O stretching mode dramatically toward the molecular long axis. The phenyl stretching transition moment direction rotates away from the molecular axis.

The computation results of the vibrational wavenumber of the OH group are also reasonably consistent with experiments, showing no peak around 3500 cm^{-1} rather a significant downshift to 3137 cm^{-1} compared with the experimental value of around 2900

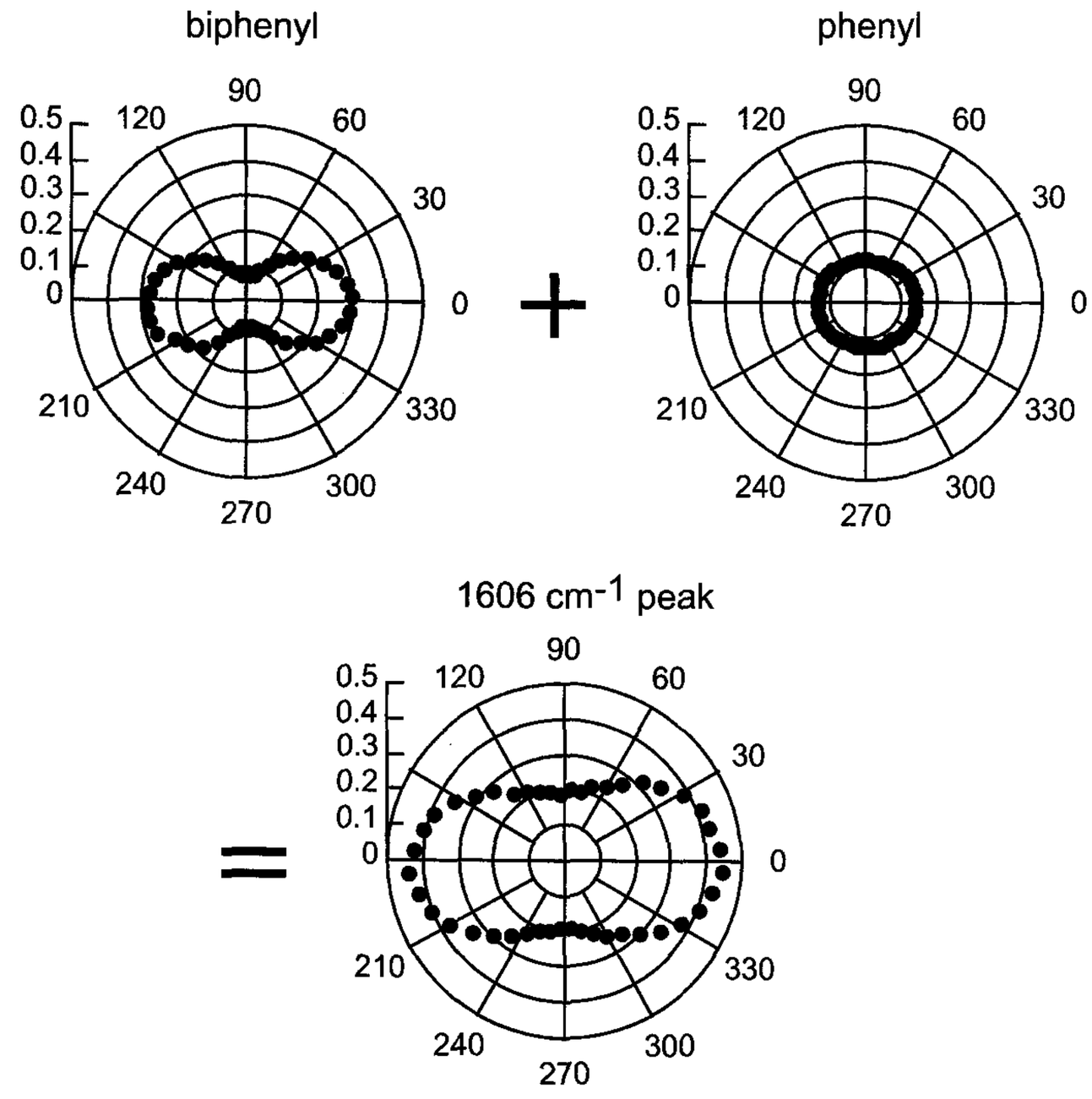

Fig. 10. The 1606 cm^{-1} profile in NTT-OH is the sum of the biphenyl (D ~ 4.25) profile and single phenyl profile which undergoes the H-bonding (D ~ 1.6).

cm^{-1}. This indicates that strong H-bonding exists, as already found in the dilution experiments. Thus, the dichroism and dilution experiments and the computations all indicate an OH - **ke** C=O *intramolecular* H- bond which is strong enough not to be broken by dilution or temperature increase.

3.2 W371 compounds

The W371 compounds also exhibit a very interesting behavior upon introduction of the NH group. The 1756 cm^{-1} C=O peak disappears and NH peaks (3370 cm^{-1}, 3347 cm^{-1}) and a new 1626 cm^{-1} peak with high D_{1626} ~ 4.91 appear. We also note that the 1736 cm^{-1} C=O dichroic ratio increases considerably from D_{1736} ~ 1.28 to D_{1736} ~ 1.53.

These effects can be largely accounted for by the calculations. Figs. 11(a,b). show the calculated low-energy conformation of the molecular fragments used to model H-bonding in the chiral tail of W371-NH. The intermolecular distance between H of NH and O of NO_2 was 1.84 Å in the optimized structure of W371 (Figs 11(a, b)), which is in the range of effective H-bonding (1.8 to 2.2 Å), and the energetics of distortion indicate a strong (~10 kCal/mole) NO_2 - NH hydrogen bond. Fig. 11(c) indicates the transition moment magnitudes and directions of the C=O and NH stretching vibrations in the low-energy conformation of the chiral tail. The amino proton was 3.21 Å away from the carbonyl oxygen, close enough for a weak NH - C=O H-bonding interaction. The calculations predict a resulting downshift in the C=O stretching vibration frequency from 1763 cm^{-1} to 1745 cm^{-1}. This downshift may account for the disappearance of the 1756 cm^{-1} **es**(NH) C=O peak upon introduction of the NH: weak H-bonding reduces its frequency to k ~1736 cm^{-1}, such that it overlaps the **es** C=O peak and increases its apparent dichroic ratio. As indicated in Fig. 12, the high dichroic ratio of the **es**(NH) C=O peak ($D_{es(NH)}$ ~ 3.5) adds together with the low dichroic ratio of the **es** C=O peak (D_{es} ~ 1.28), giving rise to a final D ~1.72.

The NH transition dipole of the NH stretching modes at 3347 and 3370 cm^{-1}, (3351 and 3367 cm^{-1} from Gaussian94) is calculated to have β_{NH} = 47°, predicting

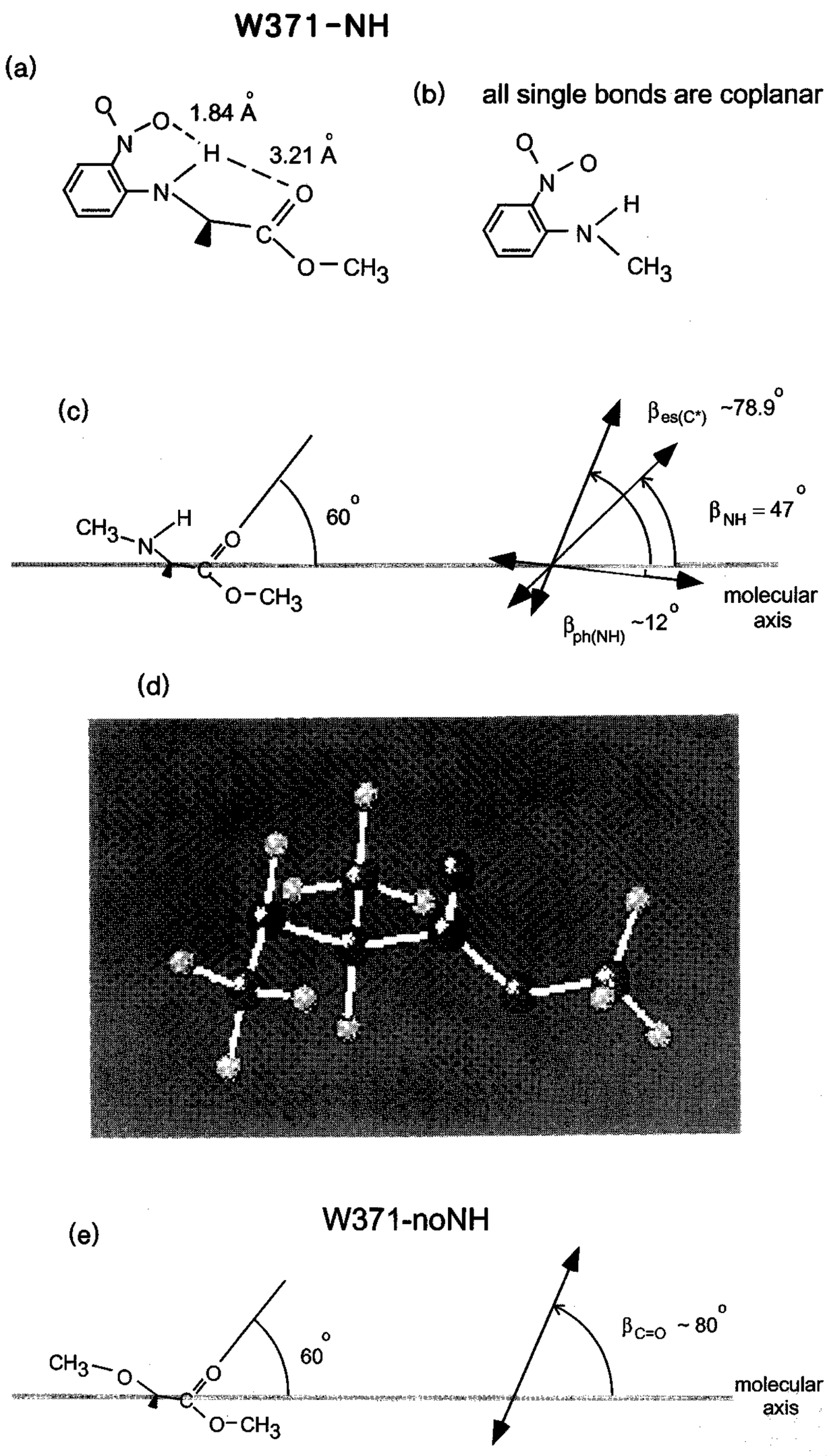

Fig. 11. Transition moment directions calculated for W371-NH and W371-noNH fragments, showing the effect of the NH substitution and NH-C=O H-bonding. (a,b) Energetically favorable NO_2, NH conformation. These interatomic distances yield a strong NO_2 - NH H-bond and a weak C=O – NH H-bond. (c) Transition moment directions and magnitudes for the C=O (| **p** $|_{C=O}$ = 0.233 Debye) and NH (| **p** $|_{NH}$ = 0.005 Debye) groups for this fragment. (d, e) A low energy conformation for a W371-noNH fragment. With C=O transition moment direction and magnitude (| **p** $|_{C=O}$ = 0.237 Debye).

D_{NH} = 1.6 with A_{max} at $\Omega = 0°$, which compares well to the measured D_{NH} = 1.9 and 1.4. The calculations show that the phenyl with the NO_2 substituent H-bonded to the NH exhibits coupled phenyl - NO_2 - NH stretching modes at 1549, 1570, and 1617 cm^{-1} (transition dipole |**p**| = 0.2, 0.065, and 0.17 Debye respectively). Peaks are observed at 1560 cm^{-1} and 1626 cm^{-1}. The 1626 cm^{-1} peak is large with A_{max} for $\Omega = 0°$ and a large dichroic ratio, $D_{1626} \sim 4.91$. This value of D is consistent with the small $\beta_{ph(NH)} = 12°$, calculated for this coupled phenyl – NH vibration.

From the dilution experiment and based on the

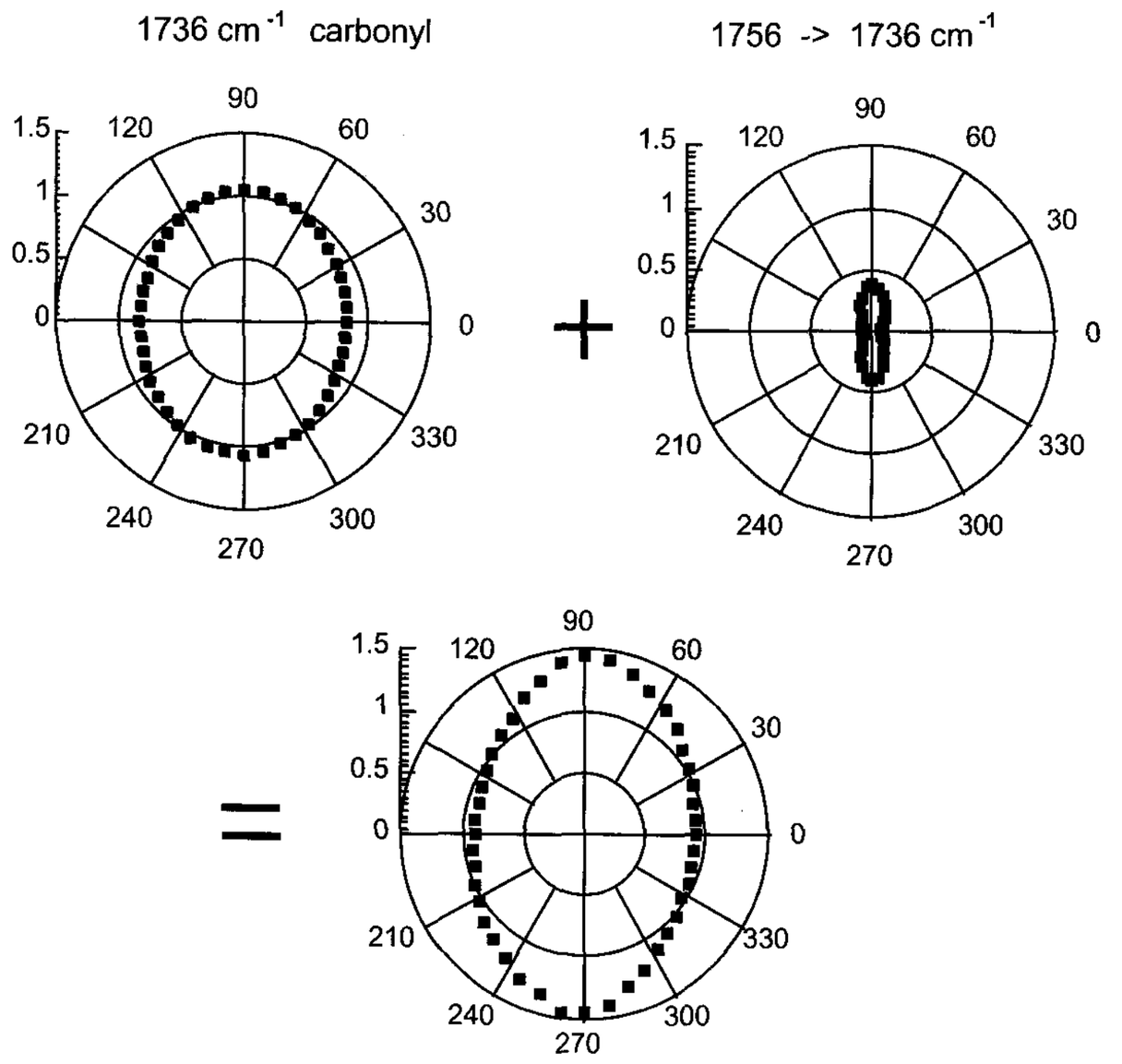

Fig. 12. The 1736 cm^{-1} C=O profile in the W371 compound is the sum of the **es** C=O (D ~1.28) and the **es**(NH) C=O profile, shifted in wavenumber from 1756 cm^{-1} to 1736 $cm^{-1}$by H-bonding.

results shown in Fig. 7, we also know that there is H-bonding, that is, weak H-bonding for the NH group (3370 cm^{-1}) and for the carbonyl group (1756 $\rightarrow$1736 cm^{-1}). Initially weak H-bonding is readily breakable from 3340 to 3370 cm^{-1} as dilution continues, but the strong H-bonded NH wavenumber remains unchanged (3347 cm^{-1}) from the liquid crystal phase (~3340 cm^{-1}). Therefore, their relative peak intensities remain the same upon dilution because the portion of strong hydrogen-bonded NH and weak hydrogen-bonded NH remain unchanged, and consequently dilution just changes the average inter-molecular distances.

3.3 MCHN1 compound

Calculations for the magnitudes and directions of the transition moments of the C=O and OH stretching vibrations in the MCHN1 compound are shown in Fig. 13. Fig. 8. indicates that the H-bonded OH stretching peak wavenumber (3430 cm^{-1}) shifts up to 3450 cm^{-1} in the Sm-B phase and that the peak splits in the Sm-A phase, with a second peak appearing at 3560 cm^{-1}, a trend enhanced upon passage into the isotropic phase and indicative of a shift to higher wavenumber with weaker H-bonding. The calculations also yield a shift to higher wavenumber with weaker H-bonding, consistent with the observed behavior, although the calculated shift is smaller than the observed. The wavenumber of the **es**(OH) C=O (k_{esOH} ~ 1765 cm^{-1}) is indicative of weak OH-C=O bonding.

The calculated transition moments, shown in Fig. 13, do not change much in orientation upon H-bonding, so the D data do not provide much information about the state of H-bonding. The calculated large $\beta_{es(OH)} \sim 80^{o}$ of the **es**(OH) C=O (1765 cm^{-1}) is consistent with the high observed $D_{es(OH)}$ = 3~4, but this is quite a typical value for a phenyl –O-C=O conformation. The high D of the **es**(OH) C=O (1765 cm^{-1}) is consistent with the calculated large $\beta_{es(OH)} = 80^{o}$. The D = 2.11 of the **es** C=O peak at 1730 cm^{-1} is somewhat larger than that typically observed for **es** carbonyls (D ~ 1.3). This is probably due to the subset of molecules in which the **es**(OH) C=O is strongly H-bonded, downshifting its wavenumber to 1730 cm^{-1} and overlapping the **es** peak. Since $\beta_{es(OH)}$ is large, this overlap increases the D in the same way as shown for W371-NH in Fig. 12. The

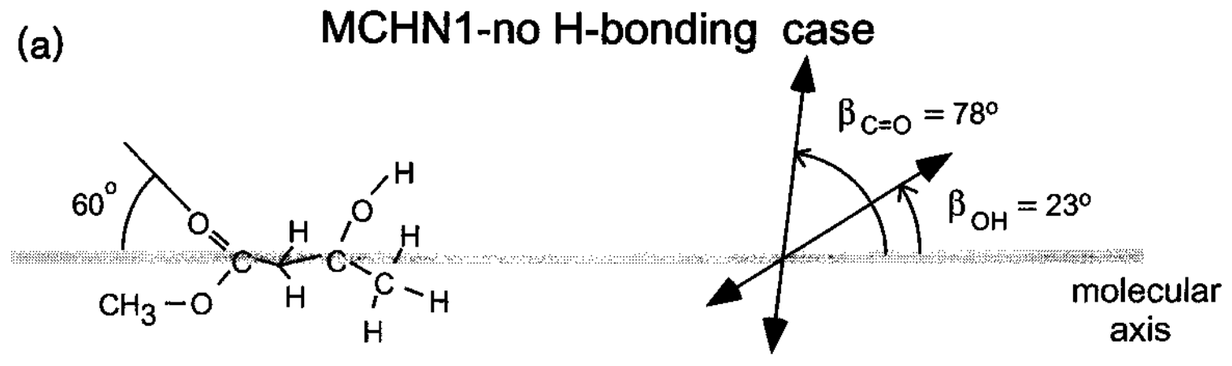

Fig. 13. Transition moment directions calculated for a MCHN1 fragment, showing the effect of OH-C=O H-bonding.

calculations have the transition moment of the OH stretching vibration nearly parallel to the molecular long axis ($\beta_{OH} < 25°$), predicting A_{max} at $\Omega = 0°$, in disagreement with the data which show essentially no dichroism ($D_{OH} \sim 1$, $\beta_{OH} = \beta_{magic} = 54.7°$) for the H-bonded OH peak and A_{max} at $\Omega = 90°$ for the non-H-bonded OH peak ($\beta_{OH} > \beta_{magic} = 54.7°$), although the increase in β_{OH} upon H-bonding is the same in both cases.

4. Conclusions

In this study, we have presented and analyzed LC materials with several distinct kinds of intramolecular H-bonding. Our principal conclusion is that currently available quantum chemical calculation tools, such as Gaussian 94 and 98, are effective for interpreting

infrared dichroism experiments in organic systems with orientational ordering of H-bonded groups. The effects of H-bonding on the vibrational transition moments are quite significant, making FTIR an effective means of studying such systems.

References

[1] R. F. Bryan, "Use of intermolecular hydrogen bonding for the induction of liquid crystallinity in the side chain of polysiloxane," J. Chem. Soc. pp. 2517-2531, 1967.

[2] M. Pfaadt, G. Moessner, D. Pressner, S. Valiyaveettil, C. Boeffel, K.Mullen, and H. W. Spiess, "Molecular order and dynamics of liquid crystals formed from Hydrogen-bonded networks of 5-Octadecyloxyisophthalic acid," J. Mater. Chem. 5, pp. 2265-2274, 1995.

[3] C. M. Paleos, and D. Tsiourvas, "Thermotropic liquid crystals formed by intermolecular hydrogen bonding interactions," Reviews Angew. Chem. Ed. Engl. 34, pp. 1696-1711, 1995.

[4] S. Ishibashi and S. Kobayashi, "New liquid-crystalline compounds with an intramolecular hydrogen bond," Liq. Cryst. 10, pp. 715-723, 1991.

[5] T. Kato, H. Adachi, A. Fujishima, and J. M. Frechet, "Self-assembly of liquid crystalline complexes having angular structures through intermolecular hydrogen bonding," Chem. Lett. 2, pp. 265-268, 1992.

[6] L. J. Yu, "Hydrogen bond-induced ferroelectric liquid crystals," Liq. Cryst. 14, pp. 1303-1309, 1993.

[7] A. Ghanem and C. Noel, "FTIR investigation of two alkyl-p-terphenyl-4,4"-dicarbonxylates in their crystalline, smectic and isotropic phases," Mol. Cryst. Liq. Cryst. 150b, pp. 447-472, 1987.

[8] Bruker FT-IR Reference Manual OPUS/IR, Version 2.0.

[9] F. Hide, N. A. Clark, K. Nito, A. Yasuda, and D. M. Walba, "Dynamic polarized infrared spectroscopy of electric field-induced molecular reoreintation in a chiral smectic-A liquid crystal," Phys. Rev. Lett. 75, pp. 2344-2349, 1995.

[10] W. G. Jang, C. S. Park, J. E. Maclennan, K. H. Kim, and N. A. Clark, "Biased rotation of carbonyl groups in chiral smectic liquid crystals," Ferroelectrics 180, pp. 213-222, 1996.

[11] Eq. 1 is exact only in absence of birefringence (optical anisotropy in the real part of the dielectric constant), when the eigenmodes of a dichroic medium are linearly polarized along the directions of maximum and minimum absorbance. For the vibrations studied here, polarized nearly along the optic axis of the real part of the dielectric constant, the birefringence can be ignored in few micron thick samples.

[12] S. Kobayashi, and S. Ishibashi, "Infrared study on the stability of the hydrogen bonding between carboxylic acid and pyridyl moieties," Mol. Cryst. Liq. Cryst. 220, pp. 1-20, 1992.

[13] R. Shao, J. Pang, N. A. Clark, J. A. Rego, and D. M. Walba, "Design and synthesis of ferroelectric liquid crystal for nonlinear optics applications," Ferroelectrics 147, pp. 255-267, 1993.

[14] K. H. Kim, K. Ishikawa, H. Takezoe, and A. Fukuda, "Orientation of alkyl chains and hindered rotation of carbonyl groups in the smectic-C* phase of anitferroelectric liquid crystals studied by polarized Fourier transform infrared spectroscopy," Phys. Rev. E 51, pp. 2166-2175, 1995.

[15] N. B. Colthup, L. H. Daly, and S. E. Wiberley, Introduction to Infrared and Raman Spectroscopy (Academic Press, New York, 1964).

[16] Gaussian94 User's Reference (Gaussian, Inc., Pittsburgh, PA, 1995).

[17] Exploring Chemistry with Electronic Structure Methods, 2nd Edition, J. B. Foresman and A. Frisch (Gaussian, Inc., Pittsburgh, 1996).

[18] C. Lee, W. Yang, and R. G. Parr, "Development of the Colle-Salvetti correction-energy formula into a functional of the electron density," Phys. Rev. B 37, pp. 785-789, 1988.

[19] A. D. Becke, "Density-functional exchange-energy approximation with correct asymptotic behavior," Phys. Rev. A 38, pp. 3098-3100, 1988 and references therein.

[20] M. Nendel, Ph.D. dissertation, University of California, Los Angeles, 1996 (unpublished).